Evaluation of the Local Chloride Concentration and the Local Mechanical Stresses in Intergranular Damages Grown on a 2024 Aluminum Alloy

Céline Larignon, Joël Alexis, Eric Andrieu, Christine Blanc, Grégory Odemer

Evaluation of the Local Chloride Concentration and the Local mechanical Stresses in Intergranular Damages Grown on a 2024 Aluminum Alloy

C. Larignon[a], J. Alexis[b], E. Andrieu[a], C. Baret-Blanc[a], and G. Odemer[a]

[a] Université de Toulouse, CIRIMAT, UPS/CNRS/INPT, 4 allée Emile Monso, BP 44362, 31030 Toulouse cedex 4, France
[b] Université de Toulouse, INP/ENIT/LGP, 47 avenue d'Azereix, BP 1629, 65016 Tarbes, France

The corrosion behavior of a 2024 T351 aluminum alloy exposed to a chloride solution was studied in the present paper. The work was focused on the effect of an environmental and thermal cyclic exposure to corrosive media and aimed to identify the main parameters explaining the changes observed between continuous and cyclic immersion tests. Optical and scanning electron microscope observations showed an increase of the intergranular corrosion damage with the extension of the corrosion from the grain boundaries to the subgrain boundaries for samples exposed to cyclic tests. An experimental set-up, including a laser beam, allowed mechanical stresses induced by the solidification of the electrolyte trapped in the corrosion damage during exposure to negative temperatures to be revealed and the chloride concentration of the electrolyte to be determined. Results were helpful in proposing corrosion mechanism during thermal and environmental cyclic exposure to chloride solutions.

Introduction

High strength aluminum alloys such as those of the 2xxx series, *e.g.* 2024-T3 alloy, are widely used in aircraft industry for the skin and wings of the aircraft even though they are susceptible to different forms of localized corrosion in chloride media such as pitting corrosion, intergranular corrosion, exfoliation and stress corrosion cracking (1-12). It is generally admitted that, in the 2xxx series alloys, intergranular corrosion is due to the presence of copper-rich intergranular precipitates in contact with a copper-poor precipitate free zone (PFZ) adjacent to the grain boundaries. Intergranular corrosion is generally associated to a preferential dissolution of the PFZ due to both galvanic coupling between the PFZ and the precipitates and between the PFZ and the matrix (6-7, 9, 13). Several factors have been identified to mainly influence both morphology and initiation and/or propagation kinetics of intergranular corrosion. The alloy metallurgical state is considered as a first order parameter. Zhang and Frankel thus identified both grain size and aspect ratio as important factors in controlling localized corrosion and especially intergranular corrosion (9, 14-15). The nature and the concentration of the aggressive media also play a significant role. An increase of the chloride concentration induces a modification of the corrosion morphology with less numerous but longer intergranular defects (14). Zhang and Frankel (9) also reported that nitrates limited the initiation and propagation processes for intergranular corrosion while sulfates reduced the density of corroded grains boundaries. Mechanical stresses highly influence localized corrosion also.

While tensile stresses seem to highly enhance the propagation rate of intergranular corrosion especially in the rolling direction, compressive stresses do not have such a significant influence even though the results are highly dependent of the electrolyte (11, 16). It has been reported that IC process is limited under compressive stresses when the electrolyte contains both chloride and sulfate ions (17). At last, the immersion conditions constitute one of the main factors implied in the localized corrosion process. Strong differences in the intergranular corrosion morphology have been evidenced depending on the conditions of exposure to aggressive media, *e.g.*, alternate immersion tests, exfoliation tests, intergranular corrosion tests (18). Nevertheless, effects of cyclic exposure to corrosive environment have not been studied in detail yet despite the fact that, actually, aircraft structures are cyclically exposed to corrosive environment: when the plane is on the tarmac, it is exposed to corrosive environment but, during a flight, there is no more corrosive exposition and, for some parts of the structure, the temperature is low, roughly -50°C, while others are maintained at room temperature. Thus, real exposition conditions correspond to environmental cycling with or without thermal cycling.

The present works aims to reproduce as close as possible real exposition conditions. Two kinds of cyclic immersion tests were performed, *i.e.*, only environmental cyclic immersion tests and both environmental and thermal cyclic immersion tests. Results were compared to those obtained with continuous immersion tests. Observations using optical and scanning electron microscopes allowed the morphology of the intergranular damage to be accurately described depending on the exposure conditions. Residual mechanical properties of the pre-corroded samples were evaluated and the influence of the exposure conditions was studied. An experimental set-up, including a laser beam, allowed mechanical stresses induced by the solidification of the electrolyte trapped in the corrosion damage during exposure to negative temperatures to be revealed and the chloride concentration of the electrolyte to be determined depending on the exposure conditions. The results helped in improving the knowledge on intergranular corrosion mechanisms.

Experimental

Materials

Corrosion investigations were performed on 2024 T351 aluminum alloy supplied in the form of a 50 mm thick rolling plate. Its composition is given in table I. The T351 temper consists of a solid-solution heat treatment at 495°C (±5°C), water quenching, straining and tempering at room temperature for four days. The material presented an elongated structure in the longitudinal direction (L) (Fig. 1(a)). Average grain sizes in longitudinal, long transverse (LT) and short transverse (ST) directions were respectively 700, 300 and 100 µm. Observations with a scanning electron microscope (SEM) and a transmission electron microscope (TEM) showed both intragranular precipitates such as Al-Cu-Mn-Fe and Al_2-Cu-Mg and intergranular precipitates (mainly Al_2-Cu-Mg and Al-Cu-Mn precipitates) (Fig. 1(b)) in good agreement with literature (6). No precipitate free zone (PFZ) was observed along the grain boundaries on the as received plate; however, it had been revealed after heat treatment. These observations were consistent with results of Zhang and Frankel (4) who showed that a PFZ was visible for a T8 temper while not for a T3 temper.

TABLE I. Chemical composition of 2024 aluminum alloy.

Alloying elements	Al	Cu	Mg	Mn	Fe	Si	Ti
Weight (%)	Base metal	4.46	1.44	0.6	0.13	0.06	0.03

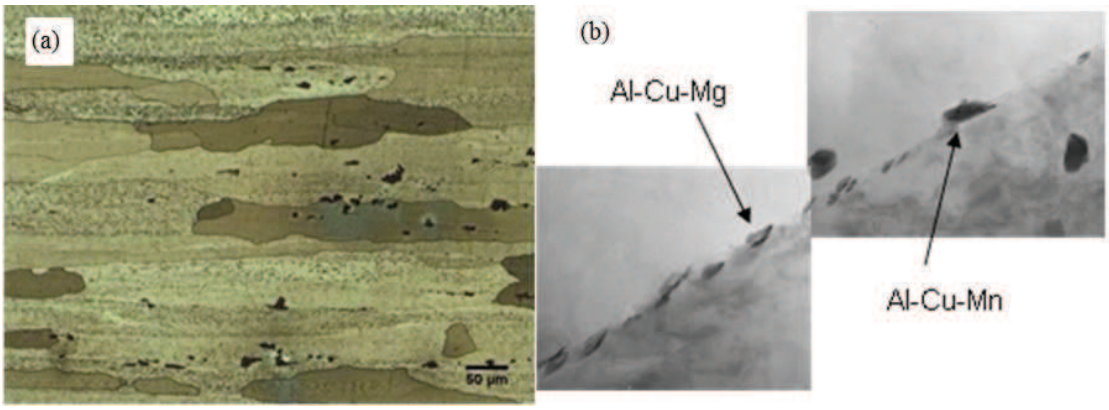

Figure 1. Microstructure of 2024 aluminum alloy (a) optical microscope observation (b) transmission microscope observation on a grain boundary.

Corrosion tests

Different immersion tests were performed to evaluate the susceptibility to intergranular corrosion of the 2024-T351 aluminum alloy with regard to immersion conditions. Tests were carried out on both cubic samples (10 mm edge, ST-LT plane exposed to the electrolyte), to observe and quantify the corrosion induced damages propagating in the L direction, and on tensile specimens (Fig. 2) to evaluate the degradation of mechanical properties due to corrosion defect propagation. All samples were removed from the core of the plate. Before immersion tests, they were polished up to 4000 grade SiC paper and then rinsed with distilled water. The electrolyte for all immersion tests consisted in a 1M NaCl solution prepared with Rectapur chemicals dissolved in distilled water. Four immersion conditions were studied with two cyclic immersion tests and two tests corresponding to continuous immersion tests. A cyclic immersion test consisted of three cycles of 24hrs; each cycle was composed of an 8hrs immersion at room temperature in the electrolyte followed by a 16h emersion in air at room temperature for CR (for Cyclic Room) test and at -20°C for CF (for Cyclic Freezing) test. The two continuous immersion tests were considered as references. The first one lasted 24hrs which corresponded to the cumulated time of immersion for cyclic immersion tests and the second one lasted 72hrs which corresponded to the duration of the whole cyclic test. Concerning the emersion temperature for CF test, preliminary measurements showed that the melting temperature of a chloride solution varied between 2°C and -16°C for chloride concentrations ranging from 0 to 5M (Fig. 3). The melting temperature was determined during the warming up of frozen solutions and an over-melting phenomenon explained the positive temperature measured for distilled water. Thermal loss certainly contributed also to explain the results. Since a 5M concentration corresponded to the maximum solubility of sodium chloride in water, it was assumed that the electrolyte trapped in the corrosion defects was frozen during the emersion step at -20°C whatever its chloride concentration. Furthermore, it was assumed that the exposure to negative temperatures of aluminum structures during an aircraft service life could

influence the corrosion behavior of the material mainly due to the solidification of the electrolyte trapped in the corrosion defects. The influence of the cooling rate was neglected so that exposure to -20°C was assumed to be representative to real aircraft conditions.

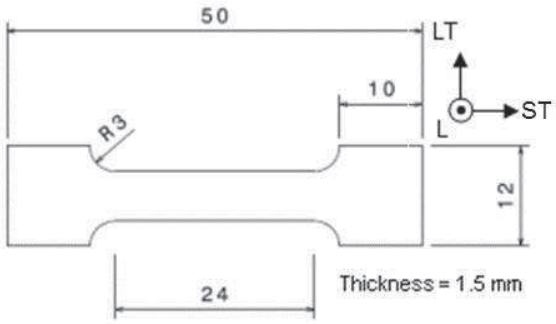

Figure 2. Schema of tensile specimens.

After the corrosion tests, both cubic samples and tensile specimens were thoroughly rinsed with distillated water, cleaned using an ultrasonic bath and finally dried. Each cubic sample was cut along the ST-L plane to obtain four slices; each slice was observed using an optical microscope and all the intergranular defects propagating in the L direction, *i.e.* perpendicularly to the ST direction, were counted and their penetration depth measured. Taking into account the cumulated length of corroded surface observed in the ST direction, *i.e.* 40 mm, and the grain size in this direction, estimated at 100 nm, almost 400 grain boundaries were analyzed for each condition of immersion tests. Four parameters were considered as relevant to describe intergranular corrosion and were statistically determined: the density of corroded grain boundaries, the average and maximal depth of intergranular defects and the cumulated length of corroded grain boundaries. The density of corroded grain boundaries corresponded to the percentage of corroded grain boundaries with regard to the total number of grain boundaries observed. The depth of penetration of an intergranular defect was measured as the distance between the samples surface and the deepest point along the corrosion defect path. The cumulated length of corroded grain boundaries was obtained by adding the length of each intergranular defect observed on the sample. Observations with a Field Gun Scanning Electron Microscope (FEG SEM) were also carried out to examine closely some defects which had been identified as unusual with regard to defect morphology generally developed during conventional immersion tests. Tensile tests were performed on tensile specimens with a MTS equipped with a 5kN cell and a constant strain rate of $10^{-3}s^{-1}$. These tests allowed the residual mechanical properties of the corroded material to be evaluated. The influence of intergranular corrosion on the mechanical properties of the alloy was estimated by comparing the values of maximal strength and elongation to failure of the corroded tensile specimens to those of an uncorroded tensile specimen.

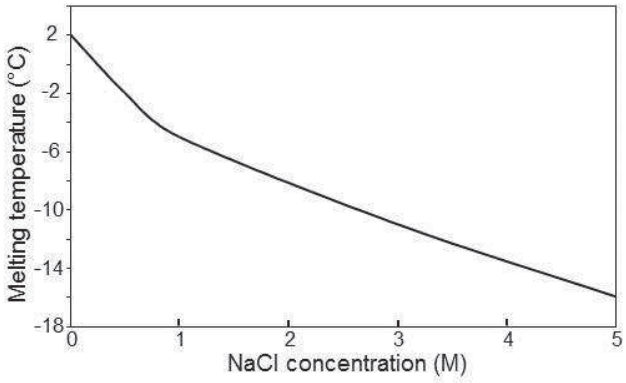

Figure 3. Melting temperature of NaCl solutions versus chloride content.

Results and discussion

Morphology of intergranular corrosion versus corrosion conditions

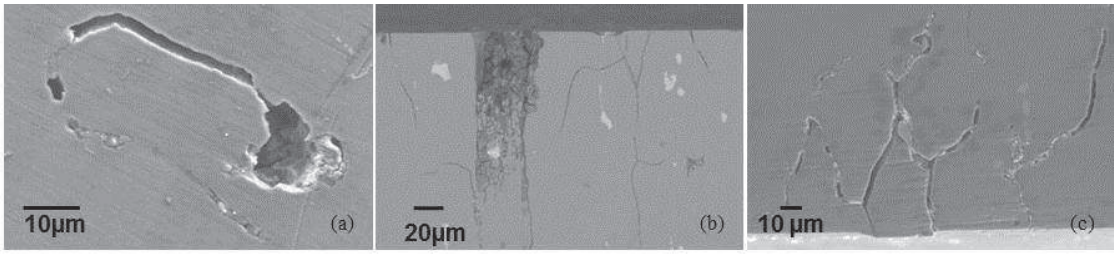

Figure 4. Representative morphology of defects developed during (a) 24h continuous immersion test, (b) cyclic immersion test at room temperature, (c) cyclic immersion test at -20°C.

Figure 4 shows FEG SEM observations of intergranular defects observed on 2024 aluminum alloy after continuous immersion tests (Fig. 4(a)), CR test (Fig. 4(b)) and CF tests (Fig 4(c)). Comparison of figure 4(a) and figures 4(b) and (c) showed that the intergranular defects developed during a cyclic corrosion test were more branched out than those formed during continuous immersion tests. Moreover, while only the grain boundaries were corroded during a continuous immersion, both grain boundaries and subgrain boundaries were found to be corroded after cyclic tests. Figure 4(b) corresponded to observations performed on a CR sample but the same results were obtained after a CF test with corrosion of subgrain boundaries but to a lesser extent. Further, to obtain a more detail description of the corrosion morphology versus the immersion conditions, all intergranular defects were observed on each sample and the morphology data (depth, number…) were statistically analyzed. Table II sums up the results obtained for the four immersion conditions. The density of corroded grain boundaries was calculated taking into account the corroded grain boundaries emerging in the ST-LT plane. Comparison of the results obtained for the 24hrs and 72hrs immersion tests showed that an increase of the immersion time led mainly to an increase of the maximal depth of the intergranular defects. No significant difference was observed concerning the density of corroded grain boundaries, the average depth and the cumulated length of the intergranular defects. The statistical analysis obtained for the

cyclic immersion tests showed that, for CR samples, the density of corroded grain boundaries, the average depth, the maximal depth and the cumulated length of intergranular defects were higher by comparison to continuous immersion tests. The distribution of the intergranular corrosion defect size was plotted to help in understanding the statistical data and results showed that CR immersion tests promoted the propagation of a few intergranular corrosion defects as well as the corrosion of subgrain boundaries as shown by FEG SEM observations. The results were different with CF immersion tests which promoted more the initiation of intergranular defects as shown by the value of the density of corroded grain boundaries. The distribution of the intergranular corrosion defect size revealed a large number of short defects which explained the average depth measured. Further, the propagation of the intergranular defect was not favoured by comparison with continuous immersion tests. Thus, while CR tests promoted the propagation of some defects, CF tests helped in initiating a large number of intergranular corrosion defects. Moreover, as said before, both cyclic tests promoted the corrosion of subgrain boundaries. The results thus showed that the morphology of intergranular corrosion was strongly influenced by the immersion conditions.

TABLE II. Statistical analysis of the data concerning the intergranular corrosion morphology for continuous and cyclic immersion tests.

Immersion tests	24 hrs	72 hrs	CR	CF
Density of corroded grain boundaries %	22.2	19.3	34.9	46.3
Average depth (µm)	59	46	111	53
Maximal depth (µm)	185	380	430	246
Cumulated length (mm)	7.9	4.6	23.5	17.1

Residual mechanical properties of corroded samples

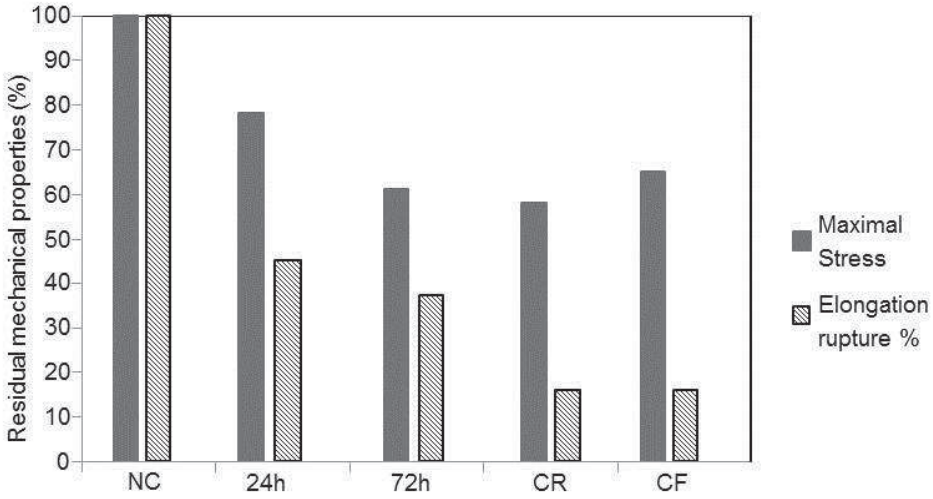

Figure 5. Residual mechanical properties of 2024 T351 aluminum alloy after continuous (24 hrs and 72hrs) and cyclic (CR and CF) immersion tests. NC corresponds to tensile tests performed on non-corroded samples.

Figure 5 shows the results of the tensile tests performed on pre-corroded specimens. Tests were also performed on non-corroded specimens and the results obtained are reported for comparison. Attention was paid to the residual maximal stress and the residual elongation to rupture of the material after immersion in chloride solutions. Results showed that immersion in chloride solutions led to a decrease of the mechanical

properties independent of the immersion conditions. Further, comparison of the residual mechanical properties obtained for 24 hrs and 72 hrs immersion tests showed that an increase of the immersion time led to a decrease of the mechanical properties *i.e.* to a more extended corrosion damage which was in good agreement with statistical data shown in table II. But the most interesting was the results obtained for CR and CF tests which showed that the maximal stress measured after the latter tests was similar to that obtained after a 72 hrs continuous immersion tests but significantly lower than that after a 24 hrs immersion tests. The elongation to rupture was dramatically reduced after both cyclic tests by comparison to the elongation to rupture measured after 24 hrs and/or 72 hrs continuous immersion tests. It seems convenient here to remain that, for cyclic tests, the immersion time was only equal to 24 hrs with 48 hrs of emersion. Moreover, additional experiments using a microbalance was carried out to determine the time the electrolyte trapped in the corrosion defects needed to evaporate during the emersion period at room temperature (CR test). Samples were first exposed to 2 cycles immersion/emersion at room temperature and then immersed again in 1M NaCl for 8 hrs. Immediately after the last immersion period, they were weighted and their weight was measured as a function of emersion time at room temperature. The corroded sample weight rapidly decreased for the first 8 hrs and then became stable which showed that 8 hrs after the beginning of the emersion period, there was no aqueous electrolyte trapped in the corrosion defects even for large corrosion damages. Thus, the total immersion time for CR tests, taking into account the time needed to evaporate the electrolyte trapped in the corrosion defects, was no more than 48 hrs which could not explain the enhanced corrosion damage compared to 72 hrs immersion tests. The hypothesis was that the chloride concentration in the electrolyte trapped in the corrosion defects could become very high due to the evaporation of water during the emersion period. Concerning the CF tests, it was assumed that the electrolyte trapped in the intergranular corrosion defects was frozen immediately on the beginning of the emersion at -20 °C due to the little size of the samples. Moreover, no electrochemical processes could occur during the emersion period at -20°C. Therefore, for this latter test, the immersion period was only equal to 24 hrs which once more could not explain the results compared to 24 and 72 hrs continuous immersion tests. For CF test, another hypothesis was proposed based on the mechanical stresses generated by the electrolyte trapped in the corrosion defects since it was frozen during the emersion period at -20°C leading to a volume increase.

Corrosion mechanisms

In order to validate these hypotheses, additional experiments were performed using an experimental device including a laser beam (Fig. 6). The first aim was to check the hypothesis formulated to explain the corrosion damage observed after CF tests *i.e.* to check whether the solidification of the electrolyte trapped inside the intergranular corrosion defects during emersion at -20°C could lead to significant mechanical stresses applied on the corrosion defect walls and top. Figure 6(a) shows a principle schema of the experimental device: 1mm thick samples were cut in the 2024 aluminum plate and submitted to an immersion test in a 1M chloride solution with one side of the sample previously protected by a varnish in order to develop corrosion defects only on the other side. After corrosion exposure, the samples were dried on their surface and dipped into liquid nitrogen in order to freeze the remaining electrolyte trapped inside intergranular corrosion defects. Due to the solidification of the electrolyte, a volume expansion occurred generating mechanical stresses inside the intergranular corrosion defects. If the

mechanical stresses were significant, they could make the sample bend since only one of the sample face was submitted to a mechanical stress. The deflection of the corroded sample could then be measured using the experimental device shown in Figure 6(b). The experimental procedure was the following: after corrosion exposure (step 2 in Fig. 6(a)), the corroded specimen was placed in a Dewar flask filled with liquid nitrogen (step 3 in Fig. 6(a)). A thermocouple probe was connected to the specimen to record its temperature. An alumina pin was attached at the top of the corroded specimen to magnify the deflection and, at the top of the alumina pin, a perfectly polished alumina reference sample was attached. A laser beam was cast on the reference sample to measure the deflection of the corroded specimen. The position zero was measured when the corroded specimen was exposed to very cold temperatures. If mechanical stresses were applied inside the corrosion defects, the sample was thus bent at the beginning of the experiment. The position of the reference sample, *i.e.* the deflection of the corroded specimen, was then recorded as the temperature became warmer. When the melting point of the electrolyte trapped in the intergranular defects was reached, the corroded specimens was no more submitted to mechanical stresses and the deflection (if there was a deflection) of the corroded specimen became equal to zero so that a sharp variation of the reference sample position was measured. If no mechanical stress was applied due to the volume expansion of the electrolyte, the position of the reference sample should remain nearly stable since dilatation phenomenon due to the temperature variation might lead to a slow and continuous variation of the reference sample position.

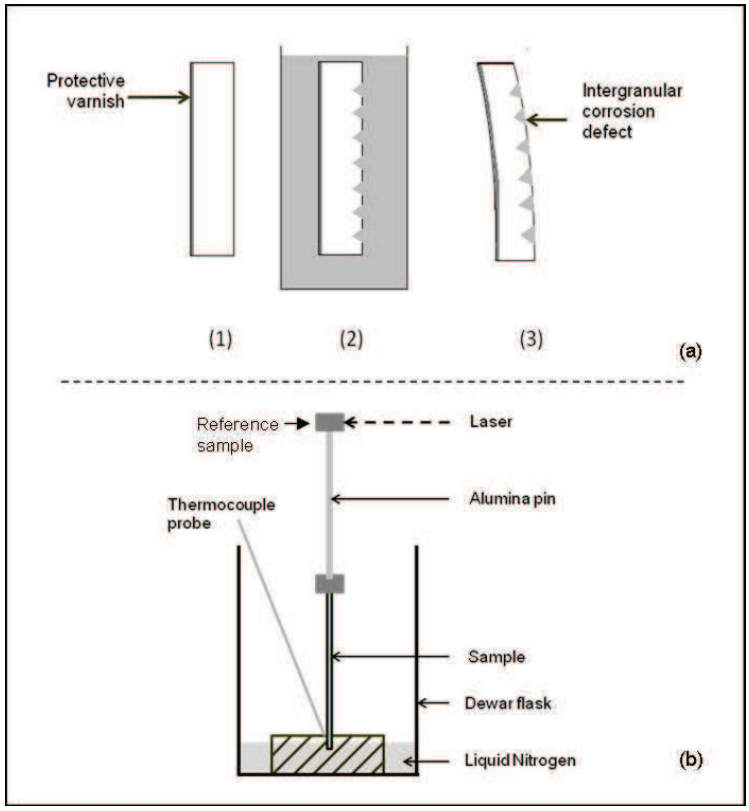

Figure 6. (a) Principle schema of the deflection experiment: 1) protection towards corrosion of the sample on one face 2) immersion tests of the sample followed by the growth of intergranular corrosion defects on the non-protected face 3) exposition of the sample to negative temperatures, solidification of the electrolyte trapped in the corrosion defects followed by the sample deflection (b) Schema of the experimental device.

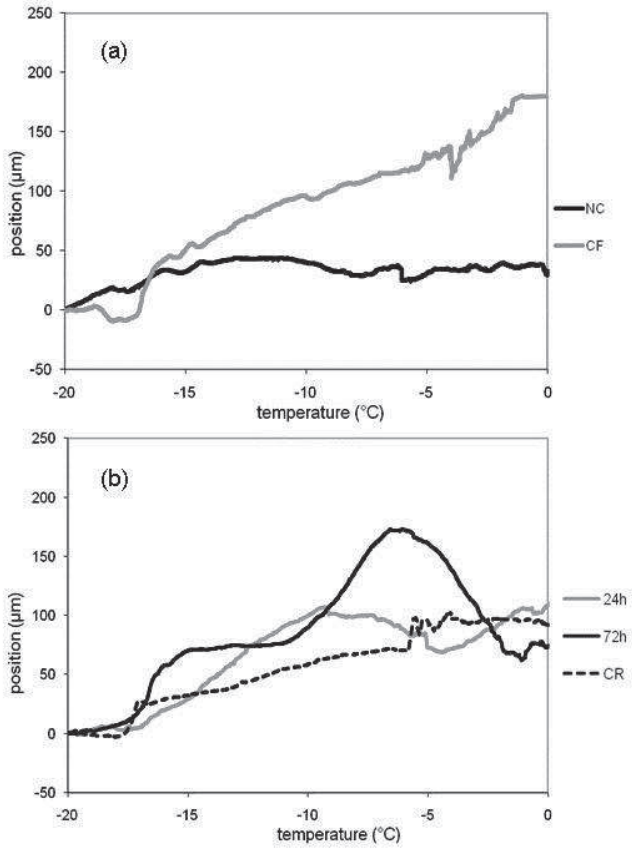

Figure 7. (a) Deflection experiments performed on a non-corroded sample and on a specimen exposed to a CF test. (b) Deflection experiments performed on a specimen exposed to a CR test and on specimens exposed to 24 and 72 hrs continuous immersion tests. For all the tests, the position of the reference sample allowed the deflection of the specimens studied to be measured as the temperature became warmer.

As said previously, experiments were first carried out to explain the corrosion behavior of samples exposed to CF tests. Figure 7(a) shows the results obtained for a sample exposed to a CF test. Results obtained for a non-corroded specimen was given for comparison. For this latter sample, the position of the alumina reference sample slowly and continuously increased when the non-corroded sample temperature increased. This measurement was related, as explained before, to dilatation phenomenon; no mechanical stress was revealed as expected. On the contrary, for the sample exposed to CF test, a sharp increase of the alumina reference sample position was observed for a temperature of -17°C. This observation showed that the sample was bent at the beginning of the deflection experiment which confirmed the hypothesis formulated to explain the corrosion damage. When 2024 aluminum alloy was submitted to a CF test, intergranular corrosion defects developed; during the emersion period at -20°C, the electrolyte trapped inside the corrosion defects solidified leading to a volume expansion significant enough to generate mechanical stresses on the walls and the top of the corrosion defects. However, the mechanical stresses were applied when the electrochemical processes were stopped due to the low temperature. Thus, the low residual mechanical properties

measured during the tensile tests (Fig. 5) could not be explained by dissolution phenomena promoted by mechanical stresses. Actually, it was first assumed that, during the immersion period, due to the anodic dissolution processes and the corresponding acidification at the corrosion defect top, hydrogen was produced. Hydrogen transport was promoted during the emersion period due to the mechanical stresses. There was thus an enriched hydrogen-zone around a corrosion defect, which size was larger than that of the corrosion defect itself. When the corroded specimens were submitted to a tensile test after the immersion test, the low mechanical properties could be partially explained by an interaction between the hydrogen-enriched zone and the dislocations generated during the tensile tests. There was thus a volume degradation of 2024 alloy during CF immersion test due to the growth of a hydrogen-enriched zone around the corrosion defects. Furthermore, it is well-known that hydrogen can weaken the chemical bonds inside a metal. Thus, during the emersion period, the opening of the corrosion defects initiated during the immersion step could be promoted by the mechanical stresses which could explain that the maximum depth of the corrosion defects was higher for CF test compared to a 24 hrs continuous immersion test (Table II). However, this effect was not probably very strong since the average depth of the corrosion defects was similar to that of a sample exposed to a 24hrs immersion. But, coupling between the weakening of the chemical bond due to the hydrogen presence and the mechanical stresses applied could explain the mechanical opening of the subgrain boundaries. The weakened subgrain boundaries would then be affected by dissolution processes during the following immersion step. Moreover, it was assumed that the mechanical stresses generated weakened the oxide film which could promote the initiation of new corrosion defects which could explain the high density of corrosion defects (Table II). Of course, the increase of corrosion defect density and the corrosion of subgrain boundaries contributed to the low residual mechanical properties measured during tensile tests for a sample exposed to CF tests as well as the existence of a volume damage related to hydrogen enrichment around the corrosion defects.

The results described above showed that the electrolyte trapped inside the corrosion defects could generate mechanical stresses strong enough to make the corroded sample bend when it was exposed to negative temperatures leading to the solidification of the electrolyte. Taking into account that the melting temperature for chloride solutions depended on the chloride concentrations (Fig. 3), it was then possible to measure the chloride content of the electrolyte trapped inside the corrosion defects using the experimental device developed (Fig. 6). Experiments were thus performed on specimens exposed to 24 and 72 hrs continuous immersion tests as well as to samples exposed to CR tests in order to determine the chloride concentration of the electrolyte trapped in the intergranular corrosion defects. The results obtained with the deflection experimental device are shown in Figure 7(b). For the samples submitted to a 72 hrs immersion test and to a CR immersion test, a sharp increase of the alumina reference sample position was measured at -17°C which allowed the chloride content inside the intergranular corrosion defects to be evaluated to 5M referring to results shown in Figure 3. On the contrary, for the samples exposed to a 24 hrs immersion tests, only a continuous increase of the reference sample position was recorded when the sample temperature was increased. Comparison of the results obtained for the non-corroded specimen (Fig. 7(a)) and for the sample exposed to a 24 hrs immersion test (Fig. 7(b)) showed that, for the latter sample, the variation of the reference sample position was higher and could not be only attributed to a dilatation phenomenon. Indeed, after a 24 hrs immersion tests,

corrosion defects were present but it was assumed that, depending on the size and the morphology of the intergranular corrosion defects, the chloride concentration varied from 5M to 1M, which corresponded to the global chloride concentration in the electrolyte. Due to this dispersion of the chloride content, a continuous increase of the reference sample position was measured when the corroded sample temperature was increased. For a sample exposed to a 72 hrs immersion test, the chloride concentration in the intergranular corrosion defects was evaluated to 5M for all the corrosion defects which showed that an increase of the immersion time led to an increase of the local chloride content in the corrosion defects. This result could partially explain the enhanced damage observed when the immersion time increased since an increase of the immersion time also promoted obviously the propagation of the corrosion defects without taking into account chloride concentration effects. Concerning samples exposed to CR tests, results thus showed that the chloride content of the electrolyte trapped in the intergranular corrosion defects was equal to 5M as well as for samples exposed to 72 hrs continuous immersion tests. It was previously shown that the density of the corrosion defects as well as their average and maximal depth were higher for samples exposed to CR tests compared to those exposed to 72 hrs immersion tests (Table II). Moreover, subgrain boundaries were found to be corroded after CR tests while no corrosion was observed on these sites after 72 hrs immersion tests. The differences were explained taking into account the results obtained by Augustin *et al.* who showed that an increase of the global chloride concentration of the electrolyte led to a decrease of the corrosion defect density with deeper defects even though an increase of the chloride concentration promoted corrosion initiation (14). This was explained by the decrease of the oxygen solubility in the electrolyte when the chloride concentration increased: only some of the intergranular defects initiated could then propagate. During a 72 hrs immersion test, the global chloride concentration of the electrolyte remained equal to 1M while the chloride concentration inside the corrosion defects reached 5M. The kinetics of the cathodic reaction, *i.e*. the oxygen reduction, was thus reduced on the corrosion defects walls due to the high chloride content but it was not limited on the sample surface. As a consequence, the density of corroded grain boundaries measured for a 72 hrs immersion test was similar to that obtained for a 24 hrs test: numerous corrosion defects could propagate and they propagated more than for a 24 hrs test due to the high chloride content inside the defects and because of the duration of the immersion test. For a CR test, during the immersion step, the chloride concentration was equal to 5M in the corrosion defects while the global concentration of the electrolyte was equal to 1M. The corrosion behavior was thus similar to that observed for a 72 hrs immersion step: it was possible to initiate numerous corrosion defects which could propagate. However, corrosion phenomena were still going on during the first 8 hrs hours of the emersion step since 8 hrs were necessary for a complete evaporation of the electrolyte inside the corrosion defects; during the emersion period, the chloride concentration was still equal to 5M in the corrosion defect and it was assumed that the chloride concentration on the sample surface progressively increased from 1M to 5M due to water evaporation and, after a time shorter than 8 hrs, there was no more electrolyte on the sample surface. So, it was convenient to distinguish two periods. When there was a thin film of electrolyte on the sample surface, it was possible to initiate new corrosion defects since there was a high chloride concentration in the surface thin film associated to a significant oxygen content related to the thickness of the electrolyte film. This led to a corrosion defect density higher than that measured for continuous immersion tests since these new corrosion defects could propagate during the emersion period and also during the following immersion period and were thus observed. However,

when the surface thin film was evaporated, the cathodic oxygen reduction only occurred on the corrosion defect walls where the chloride content was 5M. This led to an extended propagation of only some corrosion defects as shown by Augustin *et al.* (14) which explained the high value measured for the maximal depth of corrosion defects. Moreover, in the vicinity of these defects, the electrochemical conditions were so aggressive that corrosion of subgrain boundaries could occur. The combination of deep corrosion defects and subgrain boundaries corrosion probably explained the low mechanical properties measured during the following mechanical tensile tests. Of course, hydrogen could also be generated due to the anodic dissolution processes and subsequent acidification on the electrolyte trapped in the corrosion defects. But, during CR test, there was no transport and only diffusion of hydrogen in the material. As a consequence, the hydrogen-enriched zone around the corrosion defects was probably less extended compared to that grown for a sample exposed to a CF test. At last, it was worth noticing that a 5M chloride content was also measured in the corrosion defects for a CF test. But, for this latter test, the chloride concentration effect was not the main phenomenon to take into account.

Conclusions

Corrosion behavior of 2024 aluminum alloy was studied in chloride solutions. The corrosion damage observed after continuous immersion tests was compared to that observed after environmental and/or thermal cyclic tests. Results showed that cyclic corrosion tests led to an enhanced corrosion damage with corrosion of subgrain-boundaries. An experimental device was designed. It allowed mechanical stresses generated by the solidification of the electrolyte trapped inside the corrosion defects when the sample was exposed to negative temperatures to be revealed. It also allowed the chloride concentration of the electrolyte trapped to be measured. The results helped in understanding the corrosion mechanisms. For environmental cyclic tests, the enhanced corrosion damage was mainly related to chloride concentration effect while for environmental and thermal cyclic tests, mechanical stresses promoting hydrogen transport around the corrosion defects seem to be the first order factor to explain the corrosion damage.

Acknowledgments

This work was financially supported by the “Conseil Régional de la Région Midi-Pyrénées” and the “Ministère de l’Industrie” in the framework of the Diagnostat project. The authors thank S. Rolet (EADS IW) and N. Gouret (Airbus) for their help.

.

References

1. C. Blanc and G. Mankowski, *Corros. Sci.*, **40**, 411 (1998).
2. Z. Szklarska-Smialowska, *Corros. Sci.*, **41**, 1743 (1999).
3. N.D. Alexopoulos, *Mat. Sci. and Eng A.*, **520**, 48 (2009).
4. W. Zhang and G.S. Frankel, *Electrochim. Acta*, **48**, 1193 (2003).
5. J.R. Galvele, *Corros. Sci*., **47**, 3053 (2205).
6. V. Guillaumin and G. Mankowski, *Corros. Sci*., **41**, 421 (1999).
7. J.R. Galvele and S.M. De Micheli, *Corros. Sci*., **10**, 795 (1970).

8. C. Augustin, E. Andrieu, C. Blanc, G. Mankowski and J. Delfosse, *J. Electrochem. Soc*., **154**, C637 (2007).
9. W. Zhang and G.S. Frankel, *J. Electrochem. Soc*., **149**, B510 (2002).
10. M.R. Bayoumi, *Eng. Fract. Mech*., **54**, 879 (1996).
11. X. Liu, G.S. Frankel, B. Zoofan, S.I. Rokhlin, *J. Electrochem. Soc*., **153**, B42 (2006).
12. K. Urushino and K. Sugimoto, *Corros. Sci*., **19**, 225 (1978).
13. M.B. Vukmirovic, N. Dimitrov and K. Sieradski, *J. Electrochem. Soc*., **149**, B428 (2002).
14. C. Augustin, E. Andrieu, C. Baret-Blanc, J. Delfosse, G. Odemer, to be published in *J. Electrochem. Soc*.
15. D. McNaughtan, H.W. Van Rooijen, EPM. Van Westing and J.H.W. De Wit, *Corros. Sci*., **45**, 2377 (2003).
16. X. Liu, G.S. Frankel, B. Zoofan, S.I. Rokhlin, *Corros. Sci*., **46**, 405 (2004).
17. X. Liu and G.S. Frankel, *Corros. Sci.*, **48**, 3309 (2006).
18. S.G. Pantelakis, P.G. Daglaras and C.A. Apostolopoulos, *Theor. and Appl. Fract. Mech*., **33**, 117 (2000).